ACS Photonics

Article

pubs.acs.org/journal/apchd5

Red Emission of InGaN/GaN Double Heterostructures on GaN Nanopyramid Structures

Young-Ho Ko,[†,‡,§] Je-Hyung Kim,[†,§,∥] Su-Hyun Gong,[†] Joosung Kim,[⊥] Taek Kim,[⊥] and Yong-Hoon Cho*[,†]

[†]Department of Physics and KI for the NanoCentury, Korea Advanced Institute of Science and Technology (KAIST), Daejeon, 305-701, Republic of Korea

[⊥]Semiconductor Lab, Material and Device Research Center, Samsung Advanced Institute of Technology, Yongin, Gyeonggi 446-712, Republic of Korea

Supporting Information

ABSTRACT: We fabricated InGaN double-hetero structure (DHS) on the nanosized pyramid structure and successfully demonstrated efficient red color emission at 650 nm from this unique structure. The nanosized pyramid structure was fabricated by selective area growth method with nanoimprint. The different diffusion length of composite atoms and compositional pulling effect on the pyramid structure gave rise to not only compositional variation, but also high In-content InGaN of more than 40%. The InGaN DHS on nanopyramids shows high internal quantum efficiency, sub-ns fast recombination time (negligible built-in electric fields), and less efficiency droop even with the high In content. These results are important to realize efficient red emission based on InGaN material, providing possibilities for efficient photonic devices operating at the long wavelength visible region.

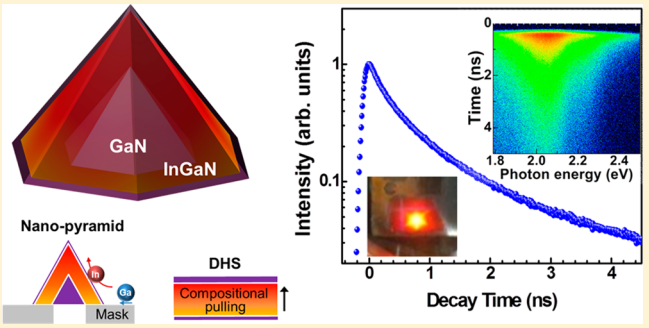

KEYWORDS: *InGaN, nanopyramid structure, red emission, heterostructure, light-emitting diode*

Beyond blue, long visible light emitting diodes (LEDs) become more important in solid-state lighting to cover all visible wavelengths. However, the efficiency of LEDs based on group III-nitrides radically decreases in long wavelengths due to the enlarged internal electric field and poor crystal quality with high In content in InGaN quantum wells (QWs).[1] Three-dimensional micro/nanostructures are promising candidates to overcome these problems. Generally, three-dimensional structures can increase light extraction efficiency, enlarge the emitting surface area, and relax the strain.[2−5] Furthermore, various semipolar/nonpolar facets can be introduced, which are hot issues for group III−N systems due to the huge internal electric fields in the *c*-plane.[6] Recently, various approaches have been suggested to form three-dimensional micro/nanostructures.[1,7] Vertically long micro/nanorods can be obtained by catalysis-driven,[8] self-organized,[9,10] patterned growth,[2,11] and chemical/mechanical etching methods.[12,13] The micro/nanopyramids can be formed mostly by selective area growth methods on patterned substrates.[14,15] Annular ring-shaped structures are also reported to form more multifaceted structures.[16] Of these, the pyramid structures are most attractive three-dimensional structures since the hexagonal pyramids are naturally grown by the low surface energy of the semipolar facets,[17] and thus, we can easily obtain highly crystalline, highly faceted structures. In addition, it is possible to control these structures by pattern designs, and the electrical driven devices can be also achieved with the typical LED device processing.[14,18] With these advantages, there have been numerous reports recently of micro/nanopyramid structures for efficient photonic devices. The InGaN QWs on micro/nanopyramids show bright emission with reduced built-in electric fields in semipolar facets.[19] The possibility of high In content with high crystal quality enables green and yellow luminescence from InGaN QWs on micro/nanopyramids.[11,15,18]

However, the red color is still challenging wavelength in InGaN QWs due to the limited In incorporation efficiency. Red emission can be observed only in a small portion (mostly the top region) of the micro/nanostructures,[3] molecular beam epitaxy grown vertical structures,[10,20] or In-rich clusters (InGaN quantum dots) in an InGaN layer.[21]

To improve the In incorporation efficiency, introduction of a thick InGaN layer, instead of thin QWs, can be one approach because the In incorporation efficiency is known to increase with the strain relaxation.[22−24] In addition, the thick InGaN layer is quite effective to reduce the carrier density by enlarging the active volume, and therefore, it is an efficient way to reduce the efficiency droop problem in group III-nitrides.[25,26]

Received: November 5, 2014
Published: January 26, 2015

DOI: 10.1021/ph500415c
ACS Photonics 2015, 2, 515−520

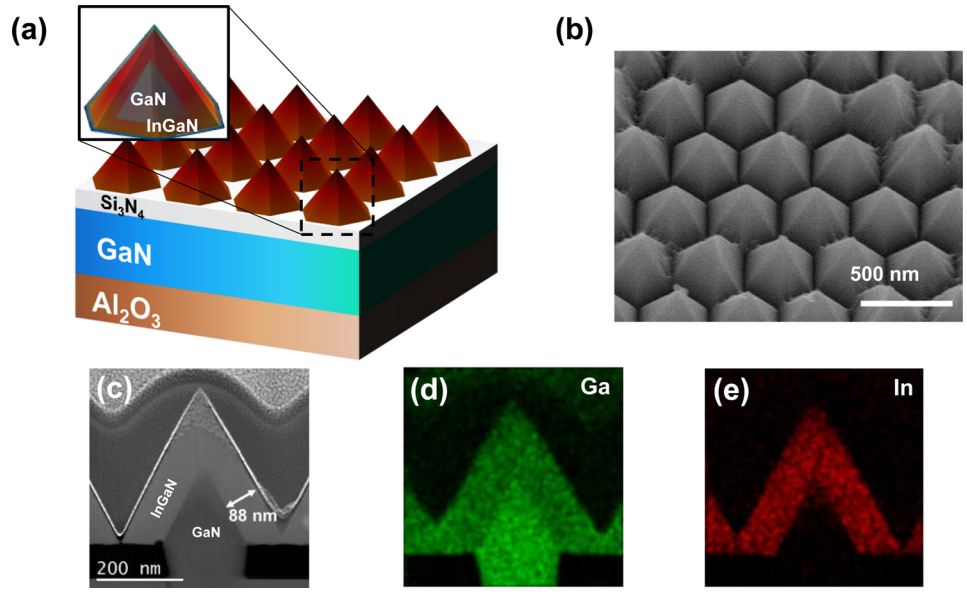

Figure 1. (a) Schematic image of InGaN DHS on GaN nanopyramids. (b) Tilted-view SEM image of a pyramid array. (c) Cross-sectional STEM image and composition mapping images for (d) Ga and (e) In atoms.

However, in general, the use of a thick InGaN layer with high In content is quite inadequate with planar structures. The high In content requires a low growth temperature, and the accumulated strain yields dislocations: therefore, the crystal quality problem arises.[27]

In this study, we combine two important structures: InGaN/GaN double heterostructures (DHSs) grown on nanosized pyramid structures. With this combination, we can eliminate the limitations of growing a thick InGaN layer and realizing high In-content InGaN and observe highly efficient red color emission from the high In-content InGaN layer. We also characterized structural and optical properties systematically, observed the formation of a high-quality InGaN thick layer, the reduction of built-in electric fields, and the improved efficiency droop.

EXPERIMENTAL DETAILS

We fabricated GaN nanopyramids formed on 2 in. patterned (0001) GaN templates by using metal−organic chemical vapor deposition (MOCVD). Circular openings with a diameter of 200 nm and a center to center pitch of 400 nm are formed by nanoimprint method on a 100 nm thick Si_3N_4 film deposited by plasma-enhanced chemical vapor deposition (PECVD). Hexagonal nanopyramid structures of GaN were selectively grown on the patterned GaN template by lateral overgrowth, followed by InGaN single layer and GaN capping layer. We used scanning electron microscopy (SEM, Hitachi-S4800) and spherical aberration-corrected scanning transmission electron microscopy (STEM, JEOL-ARM200F) to investigate the structural properties of the DHS on nanopyramids. The cross-sectional TEM samples were prepared by focused ion beam milling (FEI Helios nanolab). In composition was analyzed by point scan of energy dispersive X-ray spectroscopy (EDS, Bruker Quantax 400). To obtain time-integrated photoluminescence (PL) spectra, a 405 nm laser diode was used as an excitation source. Samples were mounted in a sample holder of a closed-cycle helium cryostat. A streak camera system (Hamamatsu) and the 390 nm second harmonic of a Ti:sapphire pulsed laser (Chameleon, Coherent) with a repetition rate of 4 MHz and a pulse width of 200 fs were used to analyze the recombination dynamics of the DHS-pyramid. Cathodoluminescence (CL) spectrum and images are obtained by a monochromator (Mono4, Gatan) attached to the field emission-SEM (XL30s, Philips).

RESULTS AND DISCUSSION

Nanosize pyramids are much more favorable than microsize pyramids since they reduce the strain more effectively and do not form dislocations.[28,29] The minimized built-in electric field in the thick InGaN layer on a pyramid structure has been theoretically studied in ref 29. Based on the GaN nanopyramids, we regrew InGaN/GaN DHSs. Figure 1a and b, respectively, shows schematic and tilted view SEM images of InGaN DHSs on GaN nanopyramids. The bottom distance between the face-to-face sidewalls of a pyramid is around 380 nm. The formation of an approximately 90 nm thick InGaN layer and a thin GaN capping layer (∼5 nm) are shown in a STEM image in Figure 1c. Figure 1d and e, respectively, shows Ga and In composition mapping images measured by EDS in STEM. The hexagonal pyramid structures have $\{11\bar{2}2\}$ semipolar facets. These semipolar facets are known to have high In incorporation efficiency.[30]

The InGaN DHS on nanopyramids has high In content around 40%, and it shows a large variation in In content depending on the position from EDS measurement. Two effects can be considered as a strong driving force of the high In content in the DHS on nanopyramids. One is the difference in the diffusion length between composite atoms,[31] and the other is the compositional pulling effect.[22−24] The In adatoms have longer vertical and lateral migration lengths compared to those of the Ga adatoms. This enables In atoms to be more effectively diffused than Ga atoms. Lateral atomic diffusion is an important growth mechanism in selective area growth method,[32] and therefore, the high In content can be obtained in nanopyramid structures. In addition, vertical diffusion induces the higher In content at the higher position of the nanopyramids, where diffusion becomes more important. Similar position-dependent In composition variation is frequently observed in several three-

DOI: 10.1021/ph500415c
ACS Photonics 2015, 2, 515−520

dimensional structures,[31,33] including the nanosized pyramid structure.[14] Another important effect is the strain relaxation in the DHS. The In atoms can be extracted out from the strained InGaN QWs to reduce the deformation energy, called the compositional pulling effect.[22] Therefore, the In incorporation efficiency is influenced by the strain of materials. The effective strain relaxation is expected in the thick InGaN layer on the nanopyramid structures, thereby lead to high In incorporation efficiency. These presumptions can be confirmed by investigating In composition and emission wavelength at various positions.

Figure 2a shows an amount of In content in InGaN DHS on nanopyramids at different vertical positions. As expected, it shows high In content at the top pyramid region (~50%) and relatively low In content at the bottom pyramid region (~30%). We also measured the In content along the growth direction at the middle height of the nanopyramid. Figure 2b shows lower In content (~30%) at the InGaN layer near GaN (the strained region), and the In content increases at the InGaN layer away from GaN (the strain relaxed region) up to 40−50%.

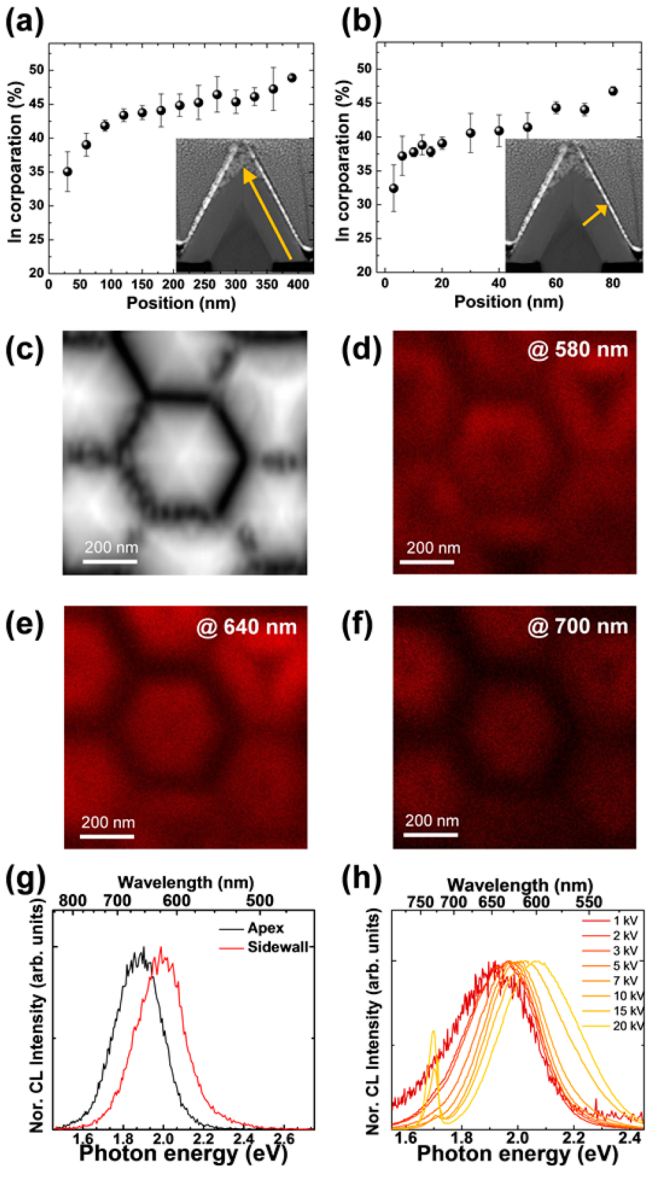

Figure 2. (a, b) Variation of In content in InGaN layer measured at various position. (a) In content variation along vertical direction. (b) In content variation along growth direction. Insets show cross-sectional TEM images for EDS measurement. (c) Top-view SEM and monochromatic CL images at (d) 580, (e) 640, and (f) 700 nm. (g) CL spectra measured at top apex and bottom side region of nanopyramids. (h) Depth-resolved CL spectra measured at various acceleration voltages.

The variation of In content depending on the position can also be confirmed from the CL experiments. Figure 2c−f shows SEM and monochromatic CL images of the DHS on nanopyramids, respectively. The monochromatic CL images show that a 580 nm wavelength is strongly emitted from the bottom side region of the nanopyramids, while a 700 nm wavelength is dominantly emitted at the top apex region of nanopyramids. The point CL spectrum in Figure 2g also shows similar trends: longer (shorter) wavelength emission at the top apex (the bottom side regions). To examine the emission energy of the InGaN layer along the growth direction, we performed CL experiments again with various acceleration voltages to obtain depth-resolved information on optical property of the InGaN layer. Figure 2h shows the peak shift of the InGaN emission toward high energy with increasing the acceleration voltage, that is, from the outer to the inner region of InGaN layer (see Figure S1 for simulation results of electron generation volume, depending on acceleration voltages). The peak at 1.7 eV shown above 7 kV is the second-order diffraction peak of GaN by a monochromator grating, indicating that the electron beam reaches the inside GaN layer. To exclude the influence of carrier density in this interpretation, such as the band filling induced blue shift, we checked the CL spectrum by changing the electron beam spot size, which changes the carrier density directly. In this experiment, the peak does not show a blue shift, regardless of carrier density. Rather, the peak shows a red shift due to the heating effect (Supporting Information, Figure S2). The above CL results match well with the EDS results and strongly support the two important mechanisms for high In content in the InGaN DHS on nanopyramid structures.

We investigated the optical properties of the InGaN DHS on nanopyramids by using various PL techniques, and the InGaN DHS on nanopyramids shows distinctive optical properties compared to the conventional planar InGaN QWs. The important figure of merit for the use of heterostructure is the crystal quality of the InGaN layer. As we grow the InGaN layer thicker, the increased strain induces the plastic relaxation of strain, that is, dislocations. The critical thickness of an InGaN film with high In content is less than 10 nm on the *c*-plane.[34] Therefore, it is difficult to expect high quantum efficiency for a planar thick InGaN layer on the *c*-plane. We measured the PL spectrum of InGaN DHS on nanopyramids with increasing temperature, as shown in Figure 3a. We also measured the InGaN DHS grown on the *c*-plane for comparison. Although the InGaN samples on both the nanopyramid and planar structures were grown at the same growth condition, the PL peak wavelength of the nanopyramid structure showed much longer wavelength (617 nm at 10 K) than the planar structure (439 nm at 10 K). The In-composition of InGaN on planar structure was measured as ~14% (much lower than that of nanopyramid structure), indicating the high In-incorporation efficiency of the nanopyramid structure. These results were well matched with our previous discussion for In-incorporation (larger diffusion length of In dominating on the mask region).

DOI: 10.1021/ph500415c
ACS Photonics 2015, 2, 515−520

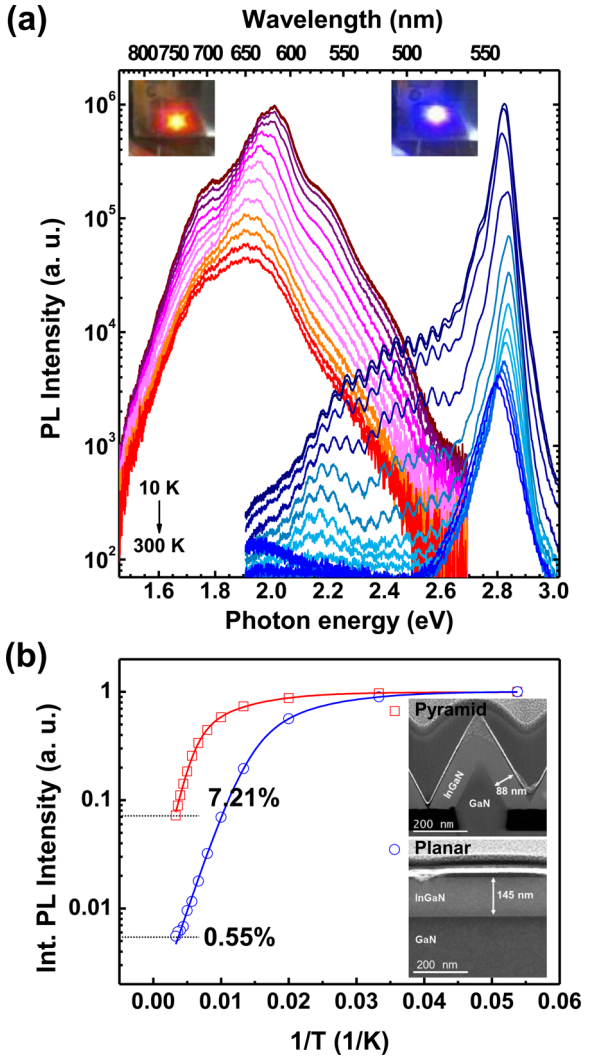

Figure 3. (a) Temperature-dependent PL spectra for the DHS on nanopyramids and the DHS-planar samples. Red (blue) curves correspond to the DHS on nanopyramids (DHS-planar). Insets show photoimages of PL emitting samples. (b) Integrated PL intensity plot as a function of temperature. Solid lines indicate fitting curves to calculate the activation energy. Insets show HADDF sTEM images of nanopyramid and planar structure.

The inset of Figure 3a are photo images showing bright red and blue PL from both samples.

Figure 3b shows the plot of the integrated PL intensity as a function of temperature. Compared to the DHS-planar, the DHS on nanopyramids show more than 10× higher PL intensity ratio between 10 and 300 K ($I_{300\ K}/I_{10\ K}$ measured as 7.21 and 0.55% for nanopyarmid and planar, respectively) despite its higher In content. The activation energy of the DHS on nanopyramids is calculated from an Arrhenius equation, $I(T) = I_0[1 + A_1 \exp(-E_1/kT) + A_2 \exp(-E_2/kT)]^{-1}$. Small intensity quenching at a low temperature regime may be associated with dissociation of weakly bound excitons to residual impurity states with a small binding energy (E_1), and both samples show similar values of E_1 = 13.3 and 10.6 meV for the DHS on nanopyramids and the DHS-planar, respectively. The dominant intensity quenching occurs at high temperature. This quenching process with the activation energy of E_2 is known to be associated with the thermal escaping of carriers from the local potential minima and capturing by the nonradiative centers, and A_2 represents the density of nonradiative recombination centers.[35] The nanopyramid and planar samples show a large difference in the exciton localization energy (E_2) and their weighting constants (A_2). The resulting values given by the best fitting curves are summarized in Table 1. The larger E_2 and the smaller A_2 indicate the deeper localized energy depth and less nonradiative center density in the DHS on nanopyramids, resulting in high PL intensity up to room temperature. The DHS on nanopyramid structures are also quite effective to minimize built-in electric fields by the strain relaxation and the use of semipolar facets. We measured the carrier recombination dynamics of a 390 nm frequency doubled Ti:sapphire *fs* pulse laser and streak camera system at 15 K. Figure 4a shows a streak image and measured decay time constants at various

Table 1. Arrhenius Equation Fitting Parameters for the DHS on Nano-Pyramid and the DHS on Planar Samples

sample	IQE	A_1	E_1 (meV)	A_2	E_2 (meV)
DHS on nanopyramid	7.2	2.8	13.3	108.6	61.4
DHS on planar	0.56	7.5	10.6	897.6	37.5

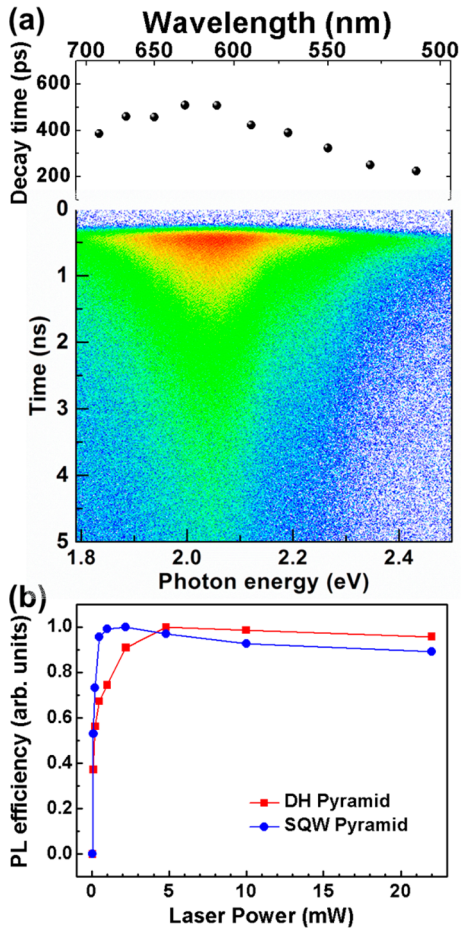

Figure 4. (a) Streak image and decay time constants at various wavelengths for the DHS on nanopyramids at 15 K. Decay time constant are obtained at 1/*e* of the initial PL intensity. (b) Comparison of efficiency droop phenomenon between the DHS on nanopyramids and the thin single QW on nanopyramid. PL efficiency (*Y*-axis) is defined as PL intensity divided by excitation powers.

DOI: 10.1021/ph500415c
ACS Photonics 2015, 2, 515−520

wavelengths. The carrier dynamics of the DHS on nanopyramids is distinctive with the typical InGaN QWs. Generally, InGaN QW has a large potential fluctuation, and a built-in electric field varies with time during the recombination. These induce a temporal spectrum shift toward low energy and a large dependence of decay time on emission wavelength.[36−38] However, the DHS on nanopyramids do not follow these behaviors. The streak image does not show a noticeable temporal spectrum shift, and the decay constants keep a similar level regardless of wavelength. The carrier density and wavelength insensitive properties indicate negligible internal electric fields in the DHS on nanopyramids. It is worth noting that the DHS on nanopyramids has subns fast time scales recombination dynamics, even at long wavelength regions. The fast radiative recombination process supports again the minimized internal electric fields in DHS on nanopyramids.

The DHS on nanopyramids shows bright red emission, high quantum efficiency, and fast recombination dynamics originated from the high crystal quality (suppressed nonradiative process) and improved oscillator strength (enhanced radiative process). These results are difficult to achieve in conventional planar structure or QW-pyramid structures. Aside from these, there is one more important merit in the DHS on nanopyramids. By using a thick active layer, it can lower carrier density in the InGaN layer. This is closely related to the efficiency droop issues at high carrier density in nitride systems. The origin of the efficiency droop is still debated and many approaches have been suggested to solve this problem,[39,40] however, lowering the carrier density is rather a direct approach for the efficiency droop problems. To investigate the role of DHS in the efficiency droop, we compared two samples: one is the InGaN DHS on nanopyramids and the other is 3 nm thick InGaN single QWs on nanopyramids. The single InGaN QW grown on nanopyramid structure was grown with the same growth condition as the InGaN DHS on nanopyramid except for the thickness of InGaN. The single InGaN QW grown on nanopyramid sample had a relatively shorter emission wavelength around 490 nm, showing the compositional pulling effect for the InGaN DHS on nanopyramid sample. We also investigated the excitation power dependent PL for InGaN DHS and single QW samples grown on nanopyramid. The InGaN DHS on nanopyramid sample had the negligible peak shift with the excitation power, while the QW on nanopyramid show a blue shift with the excitation power due to the screening of residual built-in electric field and band filling effect (Supporting Information, Figure S3). In Figure 4b, we plot the PL intensity divided by excitation power (I_{PL}/I_{exc}) as a function of excitation power (I_{exc}) at 10 K. These curves reflect the change of internal quantum efficiency (IQE) of the sample with increasing the carrier density. In the case of InGaN QW on nanopyramids, the relative IQEs rapidly increase at low power and start to decrease, while the IQEs of the DHS on nanopyramids increase slowly and show lower deceasing slope at high excitation power due to the relatively low carrier density in the DHS on nanopyramids. These results support the notion that the adoption of DHS would be quite helpful to improve efficiency droop.

CONCLUSION

In the present work, we have introduced the InGaN DHS on the nanosized pyramid structures and have successfully demonstrated efficient red color emission at 650 nm from this unique structure. Although numerous approaches have been suggested to realize red emission from an InGaN layer, bright red luminescence was difficult to achieve on the *c*-oriented planar structures and on various semipolar and nonpolar facets because of the limited In incorporation efficiency in InGaN materials. The combination of the nanopyramid and the DHS creates a synergy effect and enables high In content of more than 40%. We observed that the difference in diffusion length of composite atoms and the composition pulling effect have a crucial role for the high In content in the InGaN DHS on nanopyramids. The InGaN DHS on nanopyramids also shows high IQEs, negligible built-in electric fields, and less efficiency droop, even with the high In content. These results are important to realize efficient red emission based on InGaN material, and our suggestive approaches open new possibilities for efficient photonic devices operating at the long visible wavelength region.

ASSOCIATED CONTENT

Supporting Information

The details of the simulation for CL with various acceleration voltages, the measurement for CL with various currents, and PL spectra with changing the excitation power density. This material is available free of charge via the Internet at http://pubs.acs.org.

AUTHOR INFORMATION

Corresponding Author

*E-mail: yhc@kaist.ac.kr.

Present Addresses

[‡]The author is currently affiliated with Electronics and Telecommunications Research Institute (ETRI), 218 Gajeong-ro, Yuseong-gu, Daejeon, Korea.

[∥]The author is currently affiliated with department of Electrical and Computer Engineering, University of Maryland, College Park, Maryland 20742, U.S.A.

Author Contributions

[§]These authors contributed equally to this work (Y.-H.K. and J.-H.K.).

Notes

The authors declare no competing financial interest.

ACKNOWLEDGMENTS

This work was supported by the National Research Foundation (NRF-2013R1A2A1A01016914, NRF-2013R1A1A2011750) of the Ministry of Education, the Industrial Strategic Technology Development Program (10041878) of the Ministry of Knowledge Economy, and KAIST EEWS Initiative.

REFERENCES

(1) Crawford, M. H. LEDs for solid-state lighting: performance challenges and recent advances. *IEEE J. Sel. Top. Quantum Electron.* **2009**, *15*, 1028−1040.

(2) Yeh, T.-W.; Lin, Y.-T.; Stewart, L. S.; Dapkus, P. D.; Sarkissian, R.; O'Brien, J. D.; Ahn, B.; Nutt, S. R. InGaN/GaN multiple quantum wells grown on nonpolar facets of vertical GaN nanorod arrays. *Nano Lett.* **2012**, *12*, 3257−3262.

(3) Hong, Y. J.; Lee, C.-H.; Yoon, A.; Kim, M.; Seong, H.-K.; Chung, H. J.; Sone, C.; Park, Y. J.; Yi, G.-C. Visible-color-tunable light-emitting diodes. *Adv. Mater.* **2011**, *23*, 3284−3288.

(4) Yan, R.; Gargas, D.; Yang, P. Nanowire photonics. *Nat. Photonics* **2009**, *3*, 569−576.

(5) Li, S.; Waag, A. GaN based nanorods for solid state lighting. *J. Appl. Phys.* **2012**, *111*, 071101.

DOI: 10.1021/ph500415c
ACS Photonics 2015, 2, 515−520

(6) Masui, H.; Nakamura, S.; DenBaars, S. P.; Mishra, U. K. Nonpolar and semipolar III-nitride light-emitting diodes: achievements and challenges. *IEEE Trans. Electron Devices* **2010**, *57*, 88−100.
(7) Tsao, J. Y.; Crawford, M. H.; Coltrin, M. E.; Fischer, A. J.; Koleske, D. D.; Subramania, G. S.; Wang, G. T.; Wierer, J. J.; Karlicek, R. F. Toward smart and ultra-efficient solid-state lighting. *Adv. Opt. Mater.* **2014**, *2*, 809−836.
(8) Qian, F.; Li, Y.; Gradečak, S.; Wang, D.; Barrelet, C. J.; Lieber, C. M. Gallium nitride-based nanowire radial heterostructures for nanophotonics. *Nano Lett.* **2004**, *4*, 1975−1979.
(9) Koester, R.; Hwang, J.-S.; Salomon, D.; Chen, X.; Bougerol, C.; Barnes, J.-P.; Dang, D. L. S.; Rigutti, L.; de Luna Bugallo, A.; Jacopin, G.; Tchernycheva, M.; Durand, C.; Eymery, J. M-Plane core−shell InGaN/GaN multiple-quantum-wells on GaN wires for electroluminescent devices. *Nano Lett.* **2011**, *11*, 4839−4845.
(10) Guo, W.; Zhang, M.; Banerjee, A.; Bhattacharya, P. Catalyst-free InGaN/GaN nanowire light emitting diodes grown on (001) silicon by molecular beam epitaxy. *Nano Lett.* **2010**, *10*, 3355−3359.
(11) Riley, J. R.; Padalkar, S.; Li, Q.; Lu, P.; Koleske, D. D.; Wierer, J. J.; Wang, G. T.; Lauhon, L. J. Three-dimensional mapping of quantum wells in a GaN/InGaN core−shell nanowire light-emitting diode array. *Nano Lett.* **2013**, *13*, 4317−4325.
(12) Kim, J.-H.; Oh, C.-S.; Ko, Y.-H.; Ko, S.-M.; Park, K.-Y.; Jeong, M.; Lee, J. Y.; Cho, Y.-H. Dislocation-eliminating chemical control method for high-efficiency GaN-based light emitting nanostructures. *Cryst. Growth Des.* **2012**, *12*, 1292−1298.
(13) Li, Q.; Westlake, K. R.; Crawford, M. H.; Lee, S. R.; Koleske, D. D.; Figiel, J. J.; Cross, K. C.; Fathololoumi, S.; Mi, Z.; Wang, G. T. Optical performance of top-down fabricated InGaN/GaN nanorod light emitting diode arrays. *Opt. Express* **2011**, *19*, 25528−25534.
(14) Ko, Y.-H.; Kim, J.-H.; Jin, L.-H.; Ko, S.-M.; Kwon, B.-J.; Kim, J.; Kim, T.; Cho, Y.-H. Electrically driven quantum dot/wire/well hybrid light-emitting diodes. *Adv. Mater.* **2011**, *23*, 5364−5369.
(15) Kim, T.; Kim, J.; Yang, M.-S.; Lee, S.; Park, Y.; Chung, U.-I.; Cho, Y. Highly efficient yellow photoluminescence from {11−22} InGaN multiquantum-well grown on nanoscale pyramid structure. *Appl. Phys. Lett.* **2010**, *97*, 241111.
(16) Ko, Y.-H.; Song, J.; Leung, B.; Han, J.; Cho, Y.-H. Multi-color broadband visible light source via GaN hexagonal annular structure. *Sci. Rep.* **2014**, *4*, 5514.
(17) Sun, Q.; Yerino, C. D.; Leung, B.; Han, J.; Coltrin, M. E. Understanding and controlling heteroepitaxy with the kinetic Wulff plot: A case study with GaN. *J. Appl. Phys.* **2011**, *110*, 053517.
(18) Chang, S.-P.; Chen, Y.-C.; Huang, J.-K.; Cheng, Y.-J.; Chang, J.-R.; Sou, K.-P.; Kang, Y.-T.; Yang, H.-C.; Hsu, T.-C.; Kuo, H.-C.; Chang, C.-Y. Electrically driven nanopyramid green light emitting diode. *Appl. Phys. Lett.* **2012**, *100*, 061106.
(19) Feezell, D. F.; Speck, J. S.; DenBaars, S. P.; Nakamura, S. Semipolar (20-2-1) InGaN/GaN light-emitting diodes for high-efficiency solid-state lighting. *J. Display Technol.* **2013**, *9*, 190−198.
(20) Jahangir, S.; Mandl, M.; Strassburg, M.; Bhattacharya, P. Molecular beam epitaxial growth and optical properties of red-emitting (λ = 650 nm) InGaN/GaN disks-in-nanowires on silicon. *Appl. Phys. Lett.* **2013**, *102*, 071101.
(21) Soh, C. B.; Liu, W.; Chua, S. J.; Tan, R. J. N.; Ang, S. S.; Chow, S. Y. Red emitting LEDs formed by indium rich quantum dots incorporated in MQWs. *Phys. Status Solidi A* **2011**, *208*, 1579−1581.
(22) Pereira, S.; Correia, M. R.; Pereira, E.; O'Donnell, K. P.; Trager-Cowan, C.; Sweeney, F.; Alves, E. Compositional pulling effects in $In_xGa_{1-x}N$/GaN layers: A combined depth-resolved cathodoluminescence and Rutherford backscattering/channeling study. *Phys. Rev. B* **2001**, *64*, 205311.
(23) Hao, M.; Ishikawa, H.; Egawa, T.; Shao, C. L.; Jimbo, T. Anomalous compositional pulling effect in InGaN/GaN multiple quantum wells. *Appl. Phys. Lett.* **2003**, *82*, 4702−4704.
(24) Tsai, W.-C.; Hsu, C.-H.; Fu, S.-F.; Lee, F.-W.; Chen, C.-Y.; Chou, W.-C.; Chen, W.-K.; Chang, W.-H. Optical properties associated with strain relaxations in thick InGaN epitaxial films. *Opt. Express* **2014**, *22*, A416−A424.
(25) Gardner, N. F.; Müller, G. O.; Shen, Y. C.; Chen, G.; Watanabe, S.; Götz, W.; Krames, M. R. Blue-emitting InGaN−GaN double-heterostructure light-emitting diodes reaching maximum quantum efficiency above 200 A/cm^2. *Appl. Phys. Lett.* **2007**, *91*, 243506.
(26) Li, Y.-L.; Huang, Y.-R.; Lai, Y.-H. Efficiency droop behaviors of InGaN/GaN multiple-quantum-well light-emitting diodes with varying quantum well thickness. *Appl. Phys. Lett.* **2007**, *91*, 181113.
(27) Yam, F. K.; Hassan, Z. InGaN: An overview of the growth kinetics, physical properties and emission mechanisms. *Superlattices Microstruct.* **2008**, *43*, 1−23.
(28) Colby, R.; Liang, Z.; Wildeson, I. H.; Ewoldt, D. A.; Sands, T. D.; García, R. E.; Stach, E. A. Dislocation filtering in GaN nanostructures. *Nano Lett.* **2010**, *10*, 1568−1573.
(29) Liang, Z.; Wildeson, I. H.; Colby, R.; Ewoldt, D. A.; Zhang, T.; Sands, T. D.; Stach, E. A.; Benes, B.; García, R. E. Built-in electric field minimization in (In, Ga) N nanoheterostructures. *Nano Lett.* **2011**, *11*, 4515−4519.
(30) Northrup, J. E. GaN and InGaN(11$\bar{2}$2) surfaces: Group-III adlayers and indium incorporation. *Appl. Phys. Lett.* **2009**, *95*, 133107.
(31) Zhang, X.; Dapkus, P. D.; Rich, D. H.; Kim, I.; Kobayashi, J. T.; Kobayashi, N. P. J. InGaN/GaN quantum well growth on pyramids of epitaxial lateral overgrown GaN. *Electron. Mater.* **2000**, *29*, 10−14.
(32) Sakata, Y.; Inomoto, Y.; Komatsu, K. Surface migration effect and lateral vapor-phase diffusion effect for InGaAsP/InP narrow-stripe selective metal-organic vapor-phase epitaxy. *J. Cryst. Growth* **2000**, *208*, 130−136.
(33) Pérez-Solórzano, V.; Gröning, A.; Jetter, M.; Riemann, T.; Christen. Near-red emission from site-controlled pyramidal InGaN quantum dots. *J. Appl. Phys. Lett.* **2005**, *87*, 163121.
(34) Leyer, M.; Stellmach, J.; Meissner, C.; Pristovsek, M.; Kneissl, M. The critical thickness of InGaN on GaN. *J. Cryst. Growth* **2008**, *310*, 4913−4915.
(35) Sun, Y.; Cho, Y.-H.; Kim, H. M.; Kang, T. W.; Kwon, S. Y.; Yoon, E. Effect of growth interruption on optical properties of In-rich InGaN/GaN single quantum well structures. *J. Appl. Phys.* **2006**, *100*, 043520.
(36) Chichibu, S. F.; Azuhata, T.; Sota, T.; Mukai, T.; Nakamura, S. Localized quantum well excitons in InGaN single-quantum-well amber light-emitting diodes. *J. Appl. Phys.* **2000**, *88*, 5153−5157.
(37) Feng, S.-W.; Cheng, Y.-C.; Chung, Y.-Y.; Yang, C. C.; Lin, Y.-S.; Hsu, C.; Ma, K.-J.; Chyi, J.-I. Impact of localized states on the recombination dynamics in InGaN/GaN quantum well structures. *J. Appl. Phys.* **2002**, *92*, 4441−4448.
(38) Kim, J.-H.; Elmaghraoui, D.; Leroux, M.; Korytov, M.; Vennéguès, P.; Jaziri, S.; Brault, J.; Cho, Y.-H. Strain- and surface-induced modification of photoluminescence from self-assembled GaN/$Al_{0.5}Ga_{0.5}N$ quantum dots: strong effect of capping layer and atmospheric condition. *Nanotechnology* **2014**, *25*, 305703.
(39) Cho, J.; Schubert, E. F.; Kim, J. K. Efficiency droop in light-emitting diodes: Challenges and countermeasures. *Laser Photonics Rev.* **2013**, *7*, 408−421.
(40) Piprek. Efficiency droop in nitride-based light-emitting diodes. *J. Phys. Status Solidi A* **2010**, *207*, 2217−2225.

DOI: 10.1021/ph500415c
ACS Photonics 2015, 2, 515−520